Cluster and constraint analysis in tetrahedron packings

Weiwei Jin, Peng Lu, Lufeng Liu, and Shuixiang Li*

Department of Mechanics and Engineering Science, College of Engineering, Peking University, Beijing 100871, China

(Received 23 January 2015; revised manuscript received 3 April 2015; published 27 April 2015)

The disordered packings of tetrahedra often show no obvious macroscopic orientational or positional order for a wide range of packing densities, and it has been found that the local order in particle clusters is the main order form of tetrahedron packings. Therefore, a cluster analysis is carried out to investigate the local structures and properties of tetrahedron packings in this work. We obtain a cluster distribution of differently sized clusters, and peaks are observed at two special clusters, i.e., dimer and wagon wheel. We then calculate the amounts of dimers and wagon wheels, which are observed to have linear or approximate linear correlations with packing density. Following our previous work, the amount of particles participating in dimers is used as an order metric to evaluate the order degree of the hierarchical packing structure of tetrahedra, and an order map is consequently depicted. Furthermore, a constraint analysis is performed to determine the isostatic or hyperstatic region in the order map. We employ a Monte Carlo algorithm to test jamming and then suggest a new maximally random jammed packing of hard tetrahedra from the order map with a packing density of 0.6337.

DOI: 10.1103/PhysRevE.91.042203 PACS number(s): 45.70.−n, 61.43.−j, 83.80.Fg

I. INTRODUCTION

The packing of tetrahedra is a fundamental and remarkable issue as tetrahedron is the simplest convex polyhedron. The packing problem can be traced back to ancient Greece [1], when Aristole wrongly believed that regular tetrahedra could fully tile space. The pursuit of the densest packing of tetrahedra is a special case in the Hilbert's eighteenth problem, which is about the building up of space with congruent shapes [2]. Unlike the other four Platonic solids (hexahedron, octahedron, dodecahedron, and icosahedron), whose densest packings should be their corresponding densest lattice packings [3,4], the densest packing of tetrahedra is still unknown. The densest lattice packing of tetrahedra proved by Hoylman [5] has a relatively low packing density $\varphi_{\max}^{\text{lattice}} = 18/49$, which is evidently not the densest packing of tetrahedra. In the past decade, a lot of work has been done to investigate the densest packing of tetrahedra, and the packing densities improved from 0.7165 to 0.8563 [1,4,6–10]. The densest known tetrahedron packing, named as dimer crystal, is composed of four tetrahedra forming two dimers per unit cell. This structure was first discovered by Kallus *et al.* [9] and then optimized to a density of 0.8563 by Chen *et al.* [10]. Interestingly, a quasicrystal approximant [8], whose density is only slightly less than that of the densest dimer crystal packing, is composed of 82 tetrahedra per unit.

For the disordered packing of tetrahedra, experimental and simulation results are in a large density range. Baker and Kudrolli [11] obtained the random close packing of tetrahedral particles with a packing density of 0.64 by experiments, while a much higher random packing density of 0.76 ± 0.02 was obtained by Jaoshvili *et al.* [12]. Recently, Neudecker *et al.* [13] presented jammed packings of frictional tetrahedra with the packing density ranging from 0.469 to 0.622, which are all hyperstatic as frictions provide more constraints than the case packed by frictionless particles. With numerical methods, a number of researches and analyses have been conducted. Latham *et al.* [14] simulated the random loose packing of tetrahedra. Li *et al.* [15] showed a random close packing of tetrahedral particles ($\varphi = 0.6817$) with a sphere assembly model. Smith *et al.* [16–18] obtained the jamming threshold density of athermal, soft tetrahedra ($\varphi = 0.62 \sim 0.64$), while Jiao *et al.* [19] proposed that the density of the maximally random jammed (MRJ) packing of hard tetrahedra is 0.763 ± 0.005. Smith *et al.* [18] explained this discrepancy from a kinetic sense, as thermalization enables packing systems to overcome barriers in the athermally jammed structures with low packing densities. A jammed and disordered glass phase of tetrahedra ($\varphi = 0.7858$) was reported by Haji-Akbari *et al.* [8]. As we can see, there are some different definitions for disordered packings and all these packings can be called random packings as their positional and orientational order is small. However, these definitions did not explain their density differences clearly, especially the density discordance in the same packing state. Further work needs to be carried out to explore the inherent nature of tetrahedron packings.

Due to the geometrical frustration of tetrahedra, the disordered packings of tetrahedra often show no obvious global orientational or positional order as quantified via certain order metrics over a large range of packing densities, and it has been found that the local order in clusters is the main order form of tetrahedron packings. In our previous work [20], we used the amount of the tetrahedra forming face-face joints (strict face-face contacts) as an order metric to distinguish different packing states, considering that little variance can be observed when using other methods, including the orientational correlation function [12,19,21], face-face correlation function [12,16,21], radial distribution function (RDF) [12,16,21], and the crystal-independent metric [19]. A face-face joint here refers to two jointed tetrahedra with a common face. The clusters in tetrahedron packings have been investigated in literature before. Smith *et al.* [17,22] evaluated the average cluster size and cluster size distribution in the mechanically stable systems near jamming they obtained. Haji-Akbari *et al.* [8,23] studied the initiation, changing, and transformation of the particles forming dimers, pentagonal dipyramids, and icosahedra during Monte Carlo compression processes. However, all these investigations were based on certain

*Corresponding author: lsx@pku.edu.cn

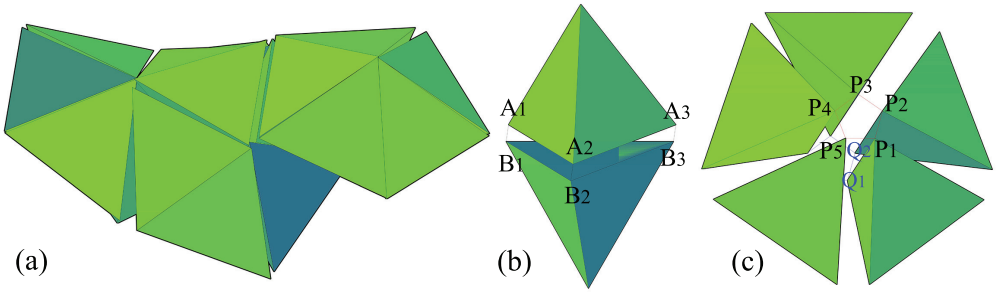

FIG. 1. (Color online) (a) A cluster of tetrahedra with a cluster size $N = 18$. (b) A face–face joint of two tetrahedra, and the distance of the two faces is enlarged. (c) A wagon wheel with five tetrahedra circling around an axis, and the distances among particles are enlarged.

packing samples and packing algorithms, and no general cluster analysis has been conducted so far to study the relationship between the cluster formation and the packing density.

In this work, we employ a cluster analysis method to further explore the local structures of tetrahedron packings. An improved relaxation algorithm, which is coupled with the hard, frictionless, and ideal tetrahedron model, is applied to provide a sufficient number of packing samples in addition to the packings obtained from literature [7,8,19]. Cluster distributions are calculated to find out if there are any special clusters in tetrahedron packings. Based on the cluster distribution results, two dominant clusters of dimer and wagon wheel are found. Therefore, we investigate the correlations between the packing density and the amounts of dimers and wagon wheels, which further prove our conclusion in Ref. [20] that the amount of face-face joints has a linear correlation with the packing density. Furthermore, a constraint analysis is performed to determine the isostaticity or hyperstaticity of tetrahedron packings. A Monte Carlo algorithm for testing jamming is then applied to check the maximally random isostatic packing obtained from the order map, and we suggest the maximally random isostatic packing as a new MRJ packing of hard tetrahedra.

II. DEFINITIONS AND METHODS

In this section, we give the definitions of clusters and particle contacts used in this work. A brief introduction of the particle model and packing algorithm are presented as well. We also introduce the definition of the order metric of ρ and the term of quasirandom packing as proposed by the authors of Ref. [20].

A. Definitions of clusters

We employ the means of cluster analysis to investigate the local structure and property of tetrahedron packings in this work, for no obvious macroscopic orientational or positional orders are observed from the fully random packing to the disordered glass phase [8] of tetrahedra. A fully random packing has no positional, orientational, or local orders. A cluster here is defined as an agglomerate of assembled particles with continuous face-face joints. Figure 1(a) shows a cluster sample with a cluster size $N = 18$. An ideal face-face joint is composed of two tetrahedra jointing each other with a common face. For the convenience of statistics, we regard two assembled tetrahedra as a face-face joint when the corresponding vertexes, as shown in Fig. 1(b), of two tetrahedra satisfy the inequality

$$\max\{||A_1B_1||,||A_2B_2||,||A_3B_3||\} < \alpha L, \tag{1}$$

where L is the edge length of the tetrahedron and α is a relative tolerance.

A strict "wagon wheel" (also know as the pentagonal dipyramid) is five tetrahedra packed around a common edge with a total 7.36° angle gap. In this work, a wagon wheel, as shown in Fig. 1(c), is defined as five assembled particles circling around an axis, and the corresponding vertexes of any two adjacent tetrahedra around the axis satisfy the following inequality

$$\max\{||P_iP_j||,||Q_iQ_j||\} < \alpha L,\ \{(i,j) = (i,i+1) \text{ and } (5,1),\ i = 1,2,3,4\} \tag{2}$$

where P_i and Q_i are the vertexes around the axis of the five tetrahedra.

B. Order metric of ρ

Global orientational and positional orders have been found to be very small in disordered tetrahedron packings which were often regarded as "random" packings. However, a large number of local order structures (clusters) have also been found indicating that these disordered packings are not fully random and the local order in clusters is the main order form in disordered tetrahedron packings. Hence, we define a relative ratio ρ to evaluate the amount of particles that forming clusters, i.e., $\rho = N_{jp}/N_p$, where N_{jp} is the number of jointed particles and N_p is the number of total particles in the packing. In our previous work [20], a strong linear correlation between the packing density and the ratio ρ was observed, which is independent of packing protocols. Thus, the ratio ρ is suggested as an order metric for measuring the order degree in tetrahedron packings.

C. Definitions of particle contacts

A constraint analysis is conducted to determine the isostaticity of tetrahedron packings in this work. If the total number of interparticle constraints of a packing system is equal to (or greater than) the total number of degrees of freedom (DOF), the system is isostatic (or hyperstatic). There are four common types of contacts in tetrahedron packings, as shown in Fig. 2, i.e., the face-to-face (F2F), edge-to-face (E2F), vertex-

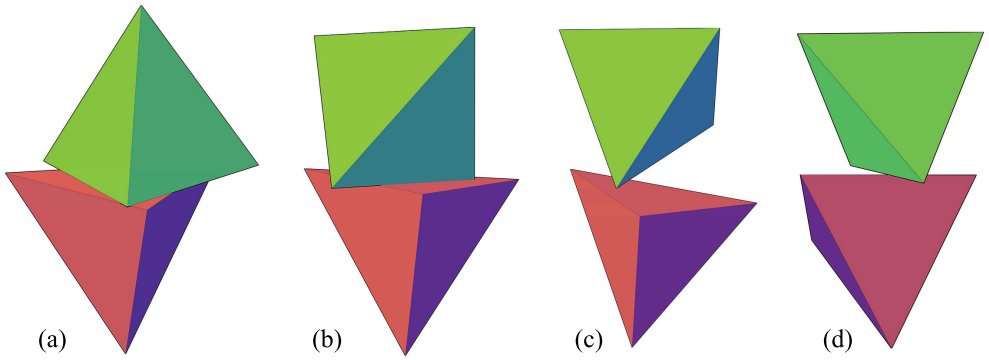

FIG. 2. (Color online) Four common types of contacts in tetrahedron packings: (a) F2F contact; (b) E2F contact; (c) V2F contact; (d) E2E contact.

to-face (V2F), and edge-to-edge (E2E) contacts, which provide three, two, one, and one constraint(s), respectively [17,19]. Details of the determination of particle contacts are described in Appendix A.

D. Particle model and relaxation algorithm

The packing algorithm employed in this work is the relaxation algorithm, which has been successfully used for the packing simulations of spherical and nonspherical particles [15,20,21,24–28]. At the beginning of a simulation, particles are randomly placed in a cubic region with a periodic boundary. The initial packing structure contains large overlaps of the particles. Then iterations of relaxation procedures are carried out to reduce the overlaps. In each procedure, both translational and rotational movements of particles are performed according to the overlaps, as described in Appendix B. The boundary expands after a certain number of iterations. When the maximum overlap rate of particles is smaller than a preset value ($<2E$-18 in this work), the simulation is terminated and the final packing is obtained. Generally, a slower expansion of the packing boundary could lead to a denser final packing. Although the relaxation algorithm is geometrically based, it is energy-driven which reduces the overlapping potential energy between particles in a kinematic way. Unlike the approximate models, i.e., the sphere assembly model [15,24–26] and spherotetrahedron model [20,21,27] used by us before, an ideal, hard, and frictionless regular tetrahedron model is applied in this work.

E. Quasirandom packing

It has been concluded that the packing of polyhedra can be sorted into four forms, i.e., the crystal, plastic crystal, liquid crystal, and fully disordered state [29,30]. However, a cluster analysis showed that considerable local order structures (or clusters) have been found in fully disordered packings of tetrahedra [20]. Hence, we proposed the concept of quasirandom packing to define the hierarchical random packing structure of clusters [20]. A quasirandom packing can be regarded as a disordered packing of building blocks of local clusters within which the particles possess cluster-induced packing order, but there is no positional or orientational order among the clusters. It is an intermediate state between the fully random state and the ordered state. The fully random packing is defined as a packing in which the particles have no positional, orientational or local orders. Figure 3 illustrates three typical states, i.e., the fully random, quasirandom, and ordered state of tetrahedral particles. The quasirandom state shows no obvious positional or orientational order, but all particles in this packing form wagon wheels.

III. RESULTS AND DISCUSSION

In this work, the relaxation algorithm coupled with the ideal tetrahedron model is applied to generate packing samples for further analysis. All these packings contain 500 congruent tetrahedra. The expansion speed of the packing space and the magnitudes of translational and rotational movements are controlled to produce samples with different packing densities and order levels. Smith *et al.* [18] investigated the effect of boundary conditions and found that variable boundaries have negligible effects on the jamming of tetrahedra. Consequently, cubic boundary conditions are mostly used in this work. In addition, the deformation of the packing boundary is also introduced to check the effect of boundary conditions. The results of cluster distributions and cluster amounts in the deforming boundary case turn out to be consistent with that in the cubic boundary case (without boundary deformation), which supports the conclusion of Smith *et al.* [18]. In this section, the properties of local structures in tetrahedron packings are investigated, and the amount of particles participating in forming dimers is suggested as an order metric. A constraint analysis is carried out to study the stability of tetrahedron packings. The isostatic and hyperstatic region is depicted in the $\varphi - \rho$ order map of tetrahedron packings. With the help of a Monte Carlo jamming test algorithm, the maximally random isostatic packing obtained in this work is confirmed to be mechanically stable and is suggested to be a new MRJ packing of hard tetrahedra.

A. Distribution of cluster forms

A larger cluster can be decomposed into different combinations of smaller ones. The statistics of cluster numbers then depends on different rules of determining the cluster. In this work, we search a packing structure from larger clusters to smaller ones to prevent repetitive statistics. Figure 4 shows the

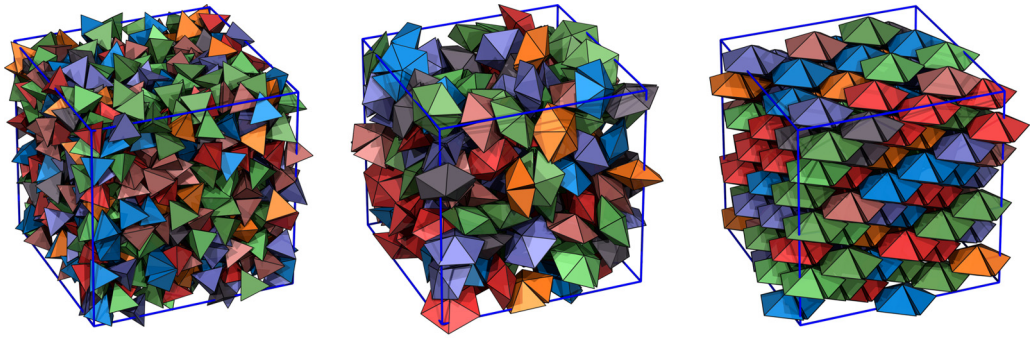

FIG. 3. (Color online) Three typical packing states of tetrahedra. (a) The fully random sate: positions and orientations of particles are random and no particles form clusters. (b) The quasirandom state: particles assemble into clusters and these clusters are packed randomly. (c) The ordered state: particles are orientationally or positionally ordered.

cluster distribution we obtained from this work as well as all available packing samples from literature [7,8,19]. The cluster distribution here represents the distribution of discrete clusters with no shared particles in packing systems. It shows the diversity of clusters from the largest ones formed in a packing system to the dissociative tetrahedra with no face-face joint. The proportion of clusters of the dimer crystal structure [10,23] is not plotted in the figure, as this packing structure has only dimers and no other cluster forms. The dimer crystal is a special case and forms from the fluid only when packing systems contain 16 or fewer particles [23].

In a probability sense, the probability of the formation of a cluster becomes smaller when the size of this cluster is larger. One would initially expect that the distribution of clusters would present a continuous decreasing trend with the increase of cluster size. However, two main peaks at $N = 2$ and $N = 5$, where N is the size of a cluster, are clearly observed in the cluster distribution diagram, and this trend is unchanged when the relative tolerance α varies. The first peak at $N = 2$ refers to the simplest cluster dimer formed by two face-face jointed tetrahedra. The clusters of the second peak at $N = 5$ are pentamers. Although the configurations of pentamers, which possess seven different types [31], are more complicated, the pentamers at the second peak are found out to be wagon wheels mostly. Despite the icosahedron-like structure [8,23] formed by 20 tetrahedra, the dimer and wagon wheel are the only two stable convex structures (or approximate convex structures with a total 7.36° angle gap) composed of tetrahedra [30]. The variation trend of the cluster distribution manifests that particles prefer to form dimers and wagon wheels to increase the stability in tetrahedron packings. This trend is believed to be associated with excluded volume. We found that the excluded volumes of dimer and wagon wheel structures are relatively lower than that of other cluster forms [31], which explains the existence of the two peaks in cluster distribution curves. Furthermore, the proportion of wagon wheels shows an overall trend of increase with the rise of packing density in Fig. 4, whereas the proportion of dimers decreases. This phenomenon is consistent with the findings in Ref. [23] that the quasicrystal approximant structure, which contains a large amount of wagon wheels, is more stable than the dimer crystal up to very high pressures.

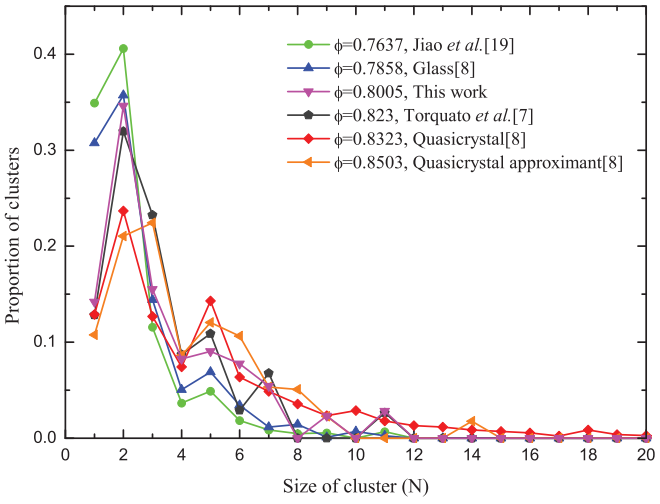

FIG. 4. (Color online) The cluster distribution of tetrahedron packings. Two peaks at $N = 2$ and $N = 5$ are observed, which are found to be dimers and wagon wheels, N is the cluster size which is the number of tetrahedra in a cluster.

The distribution of clusters indicates that the tetrahedron packings are hierarchical. Particles in tetrahedron packings prefer to form differently sized clusters. We believe that this assembling preference is a common phenomenon in particle packings, e.g., the hcp-like and fcc-like structures in sphere packings when the density is above 0.64 [32]. Consequently, it is more appropriate to use the concept of quasirandom packing to reflect the hierarchical cluster structure and to define an intermediate transition state from the fully random state to the ordered state of tetrahedron packings.

B. Dimers and wagon wheels

The distribution of clusters shows that the dimer and wagon wheel are two special and dominant cluster topologies in tetrahedron packings. We then investigate the relationship between the packing density and the relative amounts of particles forming dimers and wagon wheels, respectively. Unlike the search process above, clusters allow sharing common particles here and all particles that participate in forming dimers (or wagon wheels) are counted only once.

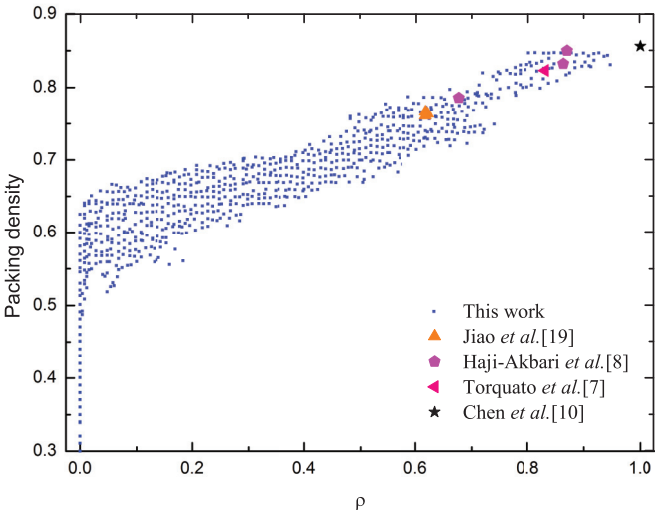

FIG. 5. (Color online) The relationship between the packing density and the relative ratio ρ, the upper bound of these points shows a nearly linear correlation, which suggests that the relative ratio ρ can be used as an order metric for tetrahedron packings.

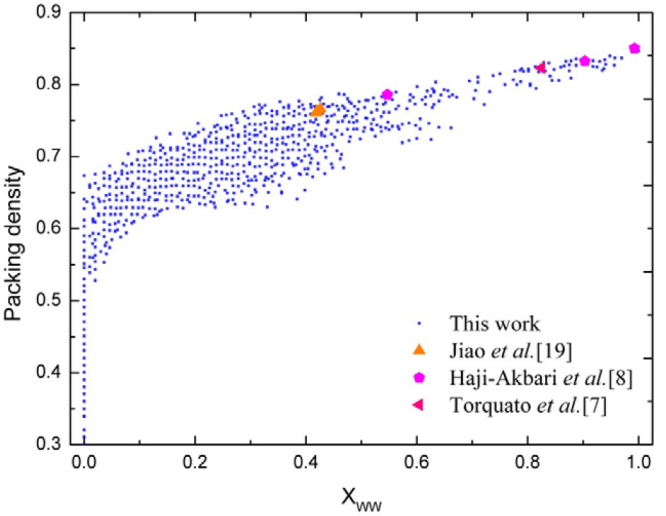

FIG. 6. (Color online) The relationship between the packing density and the relative ratio X_{ww}, the upper bound of these points shows an approximate linear correlation.

For example, when two dimers share a common tetrahedron, both of them should be regarded as dimers, and the shared tetrahedron will be used twice and counted only once. In this sense, the proportion of the relative amount of particles forming dimers is same as the definition of the order metric ρ. The relative amount of particles that forming wagon wheels is termed as X_{ww}, i.e., $X_{ww} = N_{ww}/N_p$, where N_{ww} is the number of particles that assemble into wagon wheels and N_p is the number of total particles in the packing.

We find that the value of ρ increases with α, therefore the value of α must be chosen carefully for searching clusters. An appropriate tolerance value should lead to a positive distinction among different packing states. An overly stringent threshold might cause a searching omission of slightly disturbed clusters, whereas an overly loose threshold might misidentify particles that do not form clusters. The choice of tolerances would lead to value variations of ρ and X_{ww}, but it does not affect the positive correlation between the packing density and the values of ρ and X_{ww}. Hence we select the tolerance that gives the best linearity between the upper bound of packing density and the values of ρ and X_{ww}. We then choose $\alpha = 0.07$ as the threshold for the metric ρ, which is consistent with that used in Ref. [20], and is also applied to obtain the distribution of clusters in Sec. III A.

A linear correlation between the packing density and the order metric ρ has been observed in our previous work [20]. In this work, a sufficiently large number of packing data, especially in the low packing density region, are supplemented by relaxation algorithm simulations, as shown in Fig. 5. The upper bound of the packing density versus the ratio ρ still shows a nearly linear relationship, which is consistent with our previous conclusion that this linear correlation exists on the premise that the density is the highest value for a given ρ. It demonstrates that the packing density of tetrahedron packing is determined by highly qualified face-face joints, for a face-face joint is the closest contact of two tetrahedra and more face-face joints are needed to obtain a denser packing. The packing data under the points plotted in Fig. 5 are also attainable, but in this work we only concern the high density region for a certain ρ.

We find that the upper bound of the packing density also presents an approximate linear relationship with the ratio X_{ww}, as demonstrated in Fig. 6. However, the degree of linearity between the ratio ρ and the packing density is better than that between the ratio X_{ww} and the packing density. The packing system prefers to form dimer crystal when the system size is small with 16 or fewer particles [23]. The dimer crystal-like structures contain no wagon wheels, but have relatively high packing densities (up to 0.8563). Consequently, the relative ratio ρ of dimers (face-face joints) is chosen as an order metric for tetrahedron packings, considering its linear correlation with packing density and the unification with dimer crystal-like structures, and Fig. 5 gives an $\varphi - \rho$ order map of tetrahedron packings. It shows clearly in the order map that the disordered packings in Refs. [8] and [19] have considerable local orders, and therefore they are not fully random packings.

C. Isostaticity

The isostaticity and hyperstaticity of a packing system are determined by the interparticle constraints of the system. If the total number of interparticle constraints of the packing system is equal to (or greater than) the total number of degrees of freedom (DOF), the system is isostatic (or hyperstatic). Unlike MRJ packings of ellipsoids and superballs [33,34], the MRJ packing of tetrahedra is isostatic [19]. It is necessary to identify the isostaticity of a tetrahedron packing before further discussing its jamming property. Torquato and Jiao [4,7,19] used the separating axis theorem to determine the type of interparticle contacts, while Smith *et al.* [17] used a physical interpretation of angular alignment statistics to justify cutoff values to classify contacts. Different contact counting rules may cause different classifications of particle contacts. A constraint analysis is used to determine the isostaticity (or hyperstaticity) of tetrahedron packings, as described in Appendix A. Figure 7 illustrates the relationship between

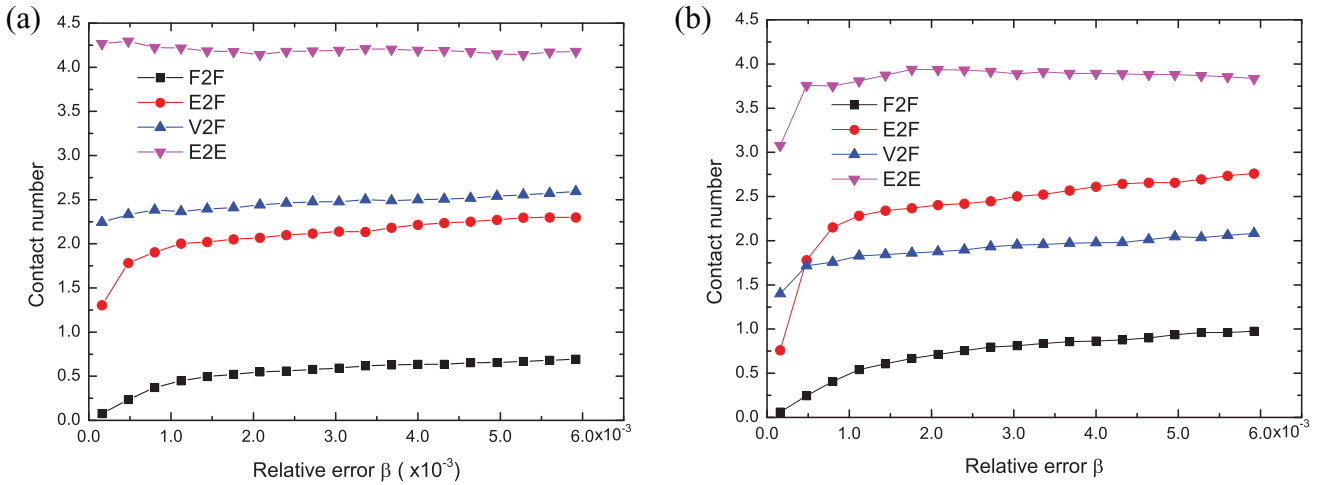

FIG. 7. (Color online) The relation between the average number of contacts per particle and the relative tolerance β, (a) the maximally random isostatic (MRI) packing in Fig. 8; (b) the jammed packing in Ref. [19]. F2F, E2F, V2F, and E2E denote the face-to-face, edge-to-face, vertex-to-face, and edge-to-edge contacts, which provide three, two, one, and one constraint(s), respectively.

the average number of contacts per particle and the relative tolerance β. The variations of the average number of contacts per particle begin to flatten when β is greater than 0.001, which indicates that the constraint analysis method used in this work is valid.

To be consistent with Ref. [19], we choose $\beta = 0.00128$, which makes the total N_{DOF} (number of the DOF constrained) of the jammed packing obtained by Jiao *et al.* [19] equal to the value 12.04 listed in their literature. Figure 5 is then redrawn to demonstrate the isostatic or hyperstatic region and the hypostatic region ($N_{\mathrm{DOF}} < 12$), as shown in Fig. 8. Note that hypostatic packings of tetrahedra still exist in the isostatic or hyperstatic region. The overlap of the two regions is reasonable, for if the boundary of a hyperstatic packing is expanded slightly and particles move relatively,

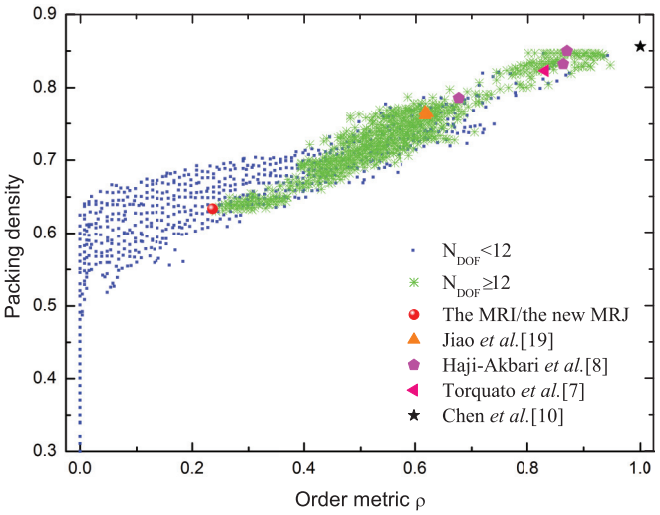

FIG. 8. (Color online) The $\varphi - \rho$ order map of tetrahedron packings, where the relative ratio ρ is used as an order metric. The isostatic and hyperstatic region is plotted with light gray (green) asterisk, and the leftmost point of the region is the maximally random isostatic packing, which is checked to be jammed.

the interparticle constraints of the packing might be broken and lead to a hypostatic packing. A special packing state, which corresponds to the point with the lowest order degree in the isostatic or hyperstatic region, can be observed in this diagram, and termed as the maximally random isostatic (MRI) packing of hard tetrahedra for its N_{DOF} (12.048) is virtually equal to the number of DOF (12.0), as listed in Table I. Note that the average number of F2F contacts of MRJ [19] calculated in this work is much smaller than that (2.21) presented in Ref. [19], and the soft jamming packings obtained by Smith *et al.* [17] exhibit approximately one F2F contact per particle. The reason for these disparities is that we apply a more strict F2F contact restriction in the constraint-counting procedure, in which the angle between the contacted faces is smaller than 0.1°. Interestingly, the density of this packing is 0.6337, which is much smaller than the MRJ packing density 0.763 ± 0.005 obtained by Jiao *et al.* [19], but close to the aforementioned jamming threshold density of athermal, soft tetrahedra ($\varphi = 0.62 \sim 0.64$, [16–18]). Notably, the packing density of the MRI packing of hard tetrahedra is slightly less than that of the MRJ packing of spheres ($\varphi \approx 0.64$). It is necessary to check the jamming property of the MRI packing for further discussion.

D. New MRJ packing of hard tetrahedra

A jamming test using Monte Carlo simulation [4,7,19] is performed to the maximally random isostatic packing obtained in this work. Jammed hard particle packing is associated with the extreme point of a jamming basin in the energy landscape.

TABLE I. The average number of contacts per particle and the total DOF constrained in the jammed packing of tetrahedra in Ref. [19] (MRJ) and in the MRI packing (MRI).

	F2F	E2F	V2F	E2E	DOF
MRJ [19]	0.572	2.328	1.824	3.844	12.04
MRI	0.48	2.008	2.384	4.208	12.048

TABLE II. The average and largest particle relative displacements, relative ratio ρ and X_{ww} of the MRI packing we obtained and the jammed packing in Ref. [19].

Packing	φ	Average relative displacement	Largest relative displacement	ρ	X_{ww}
MRJ [19]	0.7637	0.005107	0.01964	0.622	0.42
MRI	0.6337	0.006225	0.02678	0.236	0.02

Every jammed packing has a maximal allowed dilution within which transitions to other basins is impossible. Hence, if a small disturbance within the maximum dilution is given to a jammed packing artificially, the energy of the packing should swing around the jamming basin. Consequently, at the beginning of the test, the boundary of the packing region is expanded 1.01 times the boundary length L_{Cell} to open interparticle gaps, and particles inside the boundary move relatively. Afterwards, 25 000 Monte Carlo cycles are carried out for these particles, and 2000 particle trial moves are executed per Monte Carlo cycle. Each trial move can be a random translation or a random rotation with the maximal limitations of $0.1L_{\text{Cell}}$ and 0.1π, respectively. The average and largest particle relative displacements are figured out after all the MC moves. If the relative displacements are on the same magnitude of the increase scale of the boundary ($0.01L_{\text{Cell}}$), the packing can be considered jammed. Note that the jamming test method is a heuristic and approximate approach. Table II shows the comparison of the average and largest particle relative displacements between the MRI packing in this work and the jammed packing in Ref. [19]. The relative displacements are all on the same magnitude of the boundary increase for both packings. It demonstrates that the MRI packing obtained in this work is also a jammed packing with a relatively lower packing density. Considering that the local order metric ρ of the MRI packing is much less than that of the MRJ packing in Ref. [19], and the MRI and MRJ [19] packings are both jammed, we then suggest the MRI packing obtained in this work to be a new MRJ packing of hard, frictionless tetrahedra, according to the definition of MRJ.

Table I lists the average contact numbers per particle of the new MRJ packing obtained in this work and the jammed packing in Ref. [19]. It can be seen that the number of F2F contacts and E2F contacts of the new MRJ packing is less than that in Ref. [19], while the new MRJ packing possesses more V2F and E2E contacts. Indeed, F2F contacts are indispensable for strict jamming, the numbers of F2F contacts are sufficient for blocking particle rotations for both packings according the jamming test results. The new MRJ packing contains much fewer clusters, as listed in Table II, and particles forming wagon wheels in this packing are rare. It demonstrates that the new MRJ packing is more random but still in jammed state. Furthermore, the radial distribution function (RDF) curves also show disparities, as plotted in Fig. 9. There are three strong peaks in the RDF curve of the jammed packing in Ref. [19], while only two peaks with lower values appear in the curves of the new MRJ packing and the soft jammed packings [16,18]. The first three peaks in the RDF may correspond to three possible local structures as illustrated in Fig. 9. The first peak appears at the distance between two centroids of a dimer. The second peak corresponds to two nonadjacent tetrahedra (named as T_1, T_2) in a wagon wheel. If T_2 has a face-face jointed tetrahedron T_3 (not in the wagon wheel), this jointed tetrahedron T_3 and T_1 are the situation for the third peak. It can be seen that the suppression of the first two peaks and the disappearance of the last one in the RDF curves of the new MRJ packing and soft jammed packings [16,18] are caused by the lack of assembled clusters, i.e., dimers, wagon wheels, and other larger clusters. The new MRJ packing and soft jammed packings [16,18] exhibit lower local orders than the jammed packing in Ref. [19].

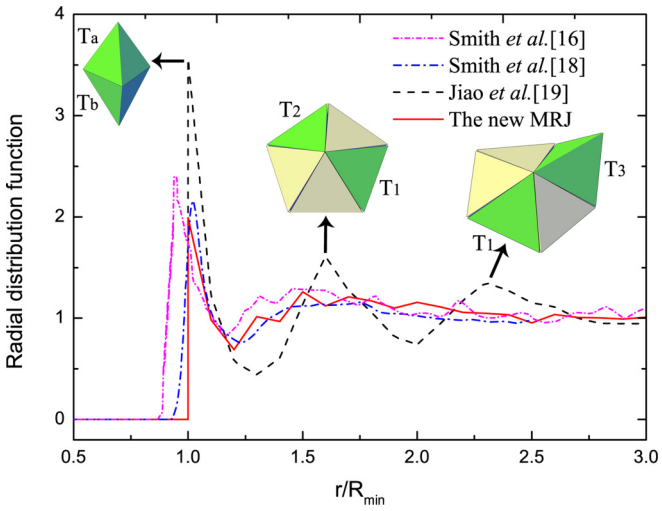

FIG. 9. (Color online) Radial distribution function (RDF) curves of the new MRJ packing, the jammed packing in Ref. [19], and soft jammed packings in Refs. [16] and [18], and three possible local structures correspond to the first three peaks in the RDF. R_{min} is the inradius of the reference tetrahedron. The three peaks appear at the distances between the two centroids of green tetrahedra (i.e., T_a and T_b, T_1 and T_2, T_1 and T_3) in the three local structures, respectively.

As mentioned above, the density of the new MRJ packing of hard tetrahedra is close to that of soft jammed tetrahedra [16,18], and the variation of the RDFs of the two packings are similar. In addition, the soft packings obtained by Smith *et al.* [16,18] are also isostatic and do exhibit lower translational order than those of the previous MRJ packings by Jiao *et al.* [19]. However, the soft jammed packings [16,18] contain overlaps between particles, which results in the nonzero values of RDF when r is smaller than R_{min} and the shift of the first peak in the RDF curves. The overlaps of the jammed packings of soft particles in Refs. [16–18] are small, but not small enough to be ignored. When the overlaps become smaller and vanish in a hard particle packing case eventually, the density of the MRJ packing should be continuous without a sharp increase or decrease from the threshold density of soft tetrahedra ($\varphi = 0.62 \sim 0.64$, [16–18]). The similarity of packing density here shows a continuous transition from soft particle packings to hard particle packings, which manifests the unity of the MRJ state for soft and hard tetrahedron packings.

IV. CONCLUSION

In summary, the improved relaxation algorithm combined with the ideal tetrahedron model is effectively applied to simulate the packing of tetrahedra from fully random state to ordered state, which supplies the foundational packing data for further analysis. In this work, a cluster analysis is employed to investigate the local structures of tetrahedron packings. The distribution of clusters shows that particles assemble into differently sized clusters especially in dense packings, and dimers and wagon wheels are two dominant cluster topologies in tetrahedron packings. The packing of tetrahedra can be then considered as a hierarchical structure of clusters. Consequently, we introduce the concept of "quasirandom packing" to further subdivide the random packing into fully random packing and quasirandom packing according to their local orders. Furthermore, the proportion of wagon wheels increases with the rise of packing density in the cluster distribution map, while the proportion of dimers decreases. It indicates that particles prefer to form dimers and wagon wheels to increase stability and more dimers further assemble into the higher level structure of wagon wheels when the packing density is high. The relative ratio ρ of face-face joints is observed to have a linear correlation with the packing density, which is suggested as a local order metric to reflect the hierarchy of clusters in tetrahedron packings. Note that the value of the relative ratio ρ is affected by the choice of tolerance. Future work needs to be done to find a more appropriate order metric, which does not depend on tolerance.

We perform a constraint analysis to determine the isostaticity (or hyperstaticity) of tetrahedron packings. Based on the order map, the isostatic and hyperstatic regions of tetrahedron packings are depicted and we obtain the maximally random isostatic (MRI) packing, which is further checked to be jammed. The MRI packing here is more random than the jammed packing in Ref. [19], as it contains fewer clusters. Hence, the MRJ packing ($\varphi = 0.6337$) we obtained is suggested to be a new MRJ packing for hard, frictionless tetrahedral particles. The packing density of this new MRJ packing is similar to the jamming threshold density of soft tetrahedra ($0.62 \sim 0.64$, [16–18]), which shows a continuous transition from soft particle packings to hard particle packings.

ACKNOWLEDGMENTS

We thank Yang Jiao for providing jammed packing configurations of hard tetrahedra and a Monte Carlo simulation code for testing jamming in hard-particle systems. This work was supported by the National Natural Science Foundation of China (Grant No. 11272010) and the National Basic Research Program of China (Grant No. 2010CB832701).

APPENDIX A: DETERMINATION OF PARTICLE CONTACTS

If the distance between two tetrahedra is smaller than a given tolerance βL, where β is a relative tolerance and L is the edge length of tetrahedra, the two tetrahedra are considered to be in contact. To determine the local contact type, the F2F contact is first checked between two tetrahedra. If the maximum distance between two faces of two different tetrahedra, is smaller than βL and the area of the projected triangle from one face to another is greater than a prescribed tolerance, the contact of the two tetrahedra is classified as a F2F contact. Then the E2F contact can be identified by analyzing if the maximum distance between one edge and one face is smaller than βL, and the projected segment from the edge to the face is intersected with the face. The V2F contact can be regarded as a special case of an E2F contact, where the edge is zero-length and this contact provides one less constraint. The remaining contacts can be then categorized into the E2E contact.

APPENDIX B: DETERMINATION OF TRANSLATION AND ROTATION IN RELAXATION PROCEDURE

Translational and rotational movements of particles are crucial in the relaxation procedure. Figure 10(a) illustrates the overlap of two tetrahedra, which is a convex polyhedron. The maximum overlap rate in a tetrahedron packing is then defined as the ratio between the maximum overlap volume among all contacted tetrahedra and the volume of a tetrahedron. To determine the directions of translational and rotational movements, a smaller ideal tetrahedron with the same center and direction is introduced as an inner core inside the tetrahedron model, as shown in Fig. 10(b). If the inner cores of two tetrahedra intersect with each other, as shown in Fig. 10(c), the directions of their translational movements is along $\mathbf{O_1O_2}$, where O_1 and O_2 are the centers of the two tetrahedra. If the two tetrahedra intersect but the inner cores do not, as shown in Fig. 10(d), the directions are along $\mathbf{P_1P_2}$, which is the shortest path between the two inner cores. The directions of rotational movements can be then obtained by setting the point of action at the center of the overlap region.

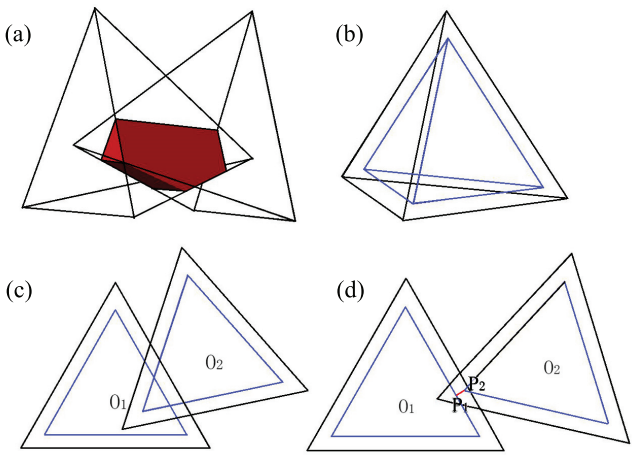

FIG. 10. (Color online) (a) The intersection of two overlapped tetrahedra is a convex polyhedron. (b) The ideal tetrahedron model with a smaller tetrahedron inside as an inner core. (c) The two-dimensional schematic diagram of two tetrahedra with inner cores intersected. (d) The two-dimensional schematic diagram of two overlapped tetrahedra with inner cores separated.

[1] E. R. Chen, Discrete Comput. Geom. **40**, 214 (2008).
[2] T. Aste and D. Weaire, *The Pursuit of Perfect Packing*, 2nd ed., (Taylor & Francis, Boca Raton, FL, 2008).
[3] U. Betke and M. Henk, Comput. Geom. **16**, 157 (2000).
[4] S. Torquato and Y. Jiao, Nature (London) **460**, 876 (2009).
[5] D. J. Hoylman, Bull. Am. Math. Soc. **76**, 135 (1970).
[6] J. H. Conway and S. Torquato, Proc. Natl. Acad. Sci. USA **103**, 10612 (2006).
[7] S. Torquato and Y. Jiao, Phys. Rev. E **80**, 041104 (2009).
[8] A. Haji-Akbari, M. Engel, A. S. Keys, X. Zheng, R. G. Petschek, P. Palffy-Muhoray, and S. C. Glotzer, Nature (London) **462**, 773 (2009).
[9] Y. Kallus, V. Elser, and S. Gravel, Discrete Comput. Geom. **44**, 245 (2010).
[10] E. R. Chen, M. Engel, and S. C. Glotzer, Discrete Comput. Geom. **44**, 253 (2010).
[11] J. Baker and A. Kudrolli, Phys. Rev. E **82**, 061304 (2010).
[12] A. Jaoshvili, A. Esakia, M. Porrati, and P. M. Chaikin, Phys. Rev. Lett. **104**, 185501 (2010).
[13] M. Neudecker, S. Ulrich, S. Herminghaus, and M. Schröter, Phys. Rev. Lett. **111**, 028001 (2013).
[14] J. P. Latham, Y. Lu, and A. Munjiza, Geotechnique **51**, 871 (2001).
[15] S. Li, J. Zhao, and X. Zhou, Chin. Phys. Lett. **25**, 1724 (2008).
[16] K. C. Smith, M. Alam, and T. S. Fisher, Phys. Rev. E **82**, 051304 (2010).
[17] K. C. Smith, T. S. Fisher, and M. Alam, Phys. Rev. E **84**, 030301 (2011).
[18] K. C. Smith, I. Srivastava, T. S. Fisher, and M. Alam, Phys. Rev. E **89**, 042203 (2014).
[19] Y. Jiao and S. Torquato, Phys. Rev. E **84**, 041309 (2011).
[20] S. Li, P. Lu, W. Jin, and L. Meng, Soft Matter **9**, 9298 (2013).
[21] J. Zhao, S. Li, W. Jin, and X. Zhou, Phys. Rev. E **86**, 031307 (2012).
[22] K. C. Smith, and T. S. Fisher, J. Heat Trans. **135**, 081301 (2013).
[23] A. Haji-Akbari, M. Engel, and S. C. Glotzer, J. Chem. Phys. **135**, 194101 (2011).
[24] S. Li, J. Zhao, P. Lu, and Y. Xie, Chin. Sci. Bull. **55**, 114 (2010).
[25] J. Zhao, S. Li, P. Lu, L. Meng, T. Li, and H. Zhu, Powder Technol. **214**, 500 (2011).
[26] L. Meng, S. Li, P. Lu, T. Li, and W. Jin, Phys. Rev. E **86**, 061309 (2012).
[27] J. Zhao, S. Li, P. Lu, R. Zou, and A. Yu, Soft Matter **8**, 1003 (2012).
[28] L. Meng, P. Lu, and S. Li, Particuology **16**, 155 (2014).
[29] J. Graaf and L. Manna, Science **337**, 417 (2012).
[30] P. F. Damasceno, M. Engel, and S.C. Glotzer, Science **337**, 453 (2012).
[31] L. Liu, P. Lu, L. Meng, W. Jin, and S. Li, Phys. Lett. A **378**, 835 (2014).
[32] B. A. Klumov, S. A. Khrapak, and G. E. Morfill, Phys. Rev. B **83**, 184105 (2011).
[33] A. Donev, I. Cisse, D. Sachs, E. A. Variano, F. H. Stillinger, R. Connelly, S. Torquato, and P. M. Chaikin, Science **303**, 990 (2004).
[34] Y. Jiao, F. H. Stillinger, and S. Torquato, Phys. Rev. E **81**, 041304 (2010).